Original Article

Investigation of Different Factors Affecting the Quality of SPECT Images: A Simulation Study

Mahsa Noori-Asl
Department of Physics, Faculty of Science, University of Mohaghegh Ardabili, Ardabil, Iran

Abstract

Background: Monte Carlo (MC) simulation codes are used extensively for modeling the nuclear medicine imaging systems, such as single photon emission computed tomography (SPECT) and positron emission tomography (PET). By using these codes, it is possible to set different imaging parameters and do various studies in the field of nuclear medicine imaging. **Aims and Objectives:** The aim of this study is to investigate the effective factors in improvement of the SPECT image quality by using MC simulation. **Materials and Methods:** In this study, we used the SIMIND MC simulation code and Jaszczak phantom containing six spheres with different diameters placed into a water-filled cylindrical phantom for consideration of the effects of different factors on quality of the images obtained from Tc-99m SPECT imaging system. The assessment criteria used to investigate these factors included image contrast, signal-to-noise ratio (SNR) and relative noise of the background (RNB). **Results:** The results of this study show that the right choice of the arc of rotation, the image matrix size, the number of angular views, type of the collimators, and also filters used in the image reconstruction affect the quality of SPECT images. Also, we show that use of scatter correction methods can improve the image quality. **Conclusion:** The MC simulation is a suitable tool for investigation of different factors affecting the quality of SPECT images, essentially in the studies based on the energy spectrum, such as the evaluation of the scatter correction methods.

Keywords: Image quality, Monte Carlo Simulation, single-photon emission computed tomography

Received on: 04-10-2019 **Review completed on:** 10-12-2019 **Accepted on:** 16-12-2019 **Published on:** 13-03-2020

Introduction

Monte Carlo (MC) simulation is a suitable and cost-effective tool for doing the different studies in the field of nuclear medicine imaging that provides a safe environment, free from the radiation exposure and hazards related to it for researchers.[1] Several MC simulation codes have been developed in the nuclear medicine imaging, including SIMSPECT[2] and SIMulation of Imaging Nuclear Detectors (SIMIND)[3] dedicated to single-photon emission computed tomography (SPECT) imaging, PETSIM,[4] Eidolon,[5] and SORTEO[6] dedicated to positron emission tomography (PET) imaging and SIMSET[7] for both imaging. Furthermore, some general-purpose codes have been developed for PET and SPECT, such as EGS4,[8] GEANT4,[9,10] and MC N-Particle Transport[11] codes.

SIMIND MC program is a dedicated simulation code for SPECT imaging. This simulation code has been developed by Michael Ljungberg in Sweden Lund University that simulates a clinical SPECT camera. By using this simulation code, it is possible to define the characteristics of the simulated imaging system. The SIMIND simulation code is included two programs, named SIMIND and CHANGE.[12] CHANGE program is included a set of indexes that by them, different parameters of imaging including detector, collimator, image, and transmission scan can be determined. However, actual MC simulation is performed by SIMIND program. This program read input files produced by CHANGE program and displays the results on the monitor. Furthermore, this program produces the results as different output files. By using SIMIND MC code, different research works have been performed in the fields of evaluation of scatter correction methods for different radioisotope sources,[13-17] attenuation

Address for correspondence: Dr. Mahsa Noori-Asl, Department of Physics, Faculty of Science, University of Mohaghegh Ardabili, Ardabil, Iran.
E-mail: nooriasl.mahsa@gmail.com

Access this article online

Quick Response Code:

Website: www.jmp.org.in

DOI: 10.4103/jmp.JMP_88_19

How to cite this article: Noori-Asl M. Investigation of different factors affecting the quality of SPECT images: A simulation study. J Med Phys 2020;45:44-51.

correction,[18] collimators,[19] radiation dosimetry,[20] and quality control.[21]

Since SPECT is one of the most commonly imaging methods used in clinical nuclear medicine, therefore, it is very important to obtain the images with the highest quality from this imaging system for diagnosis affairs, for example, to identify the precise location of tumors in oncology and also, to find the exact location of the blocked artery in cardiology. For this reason, the investigation of different factors affecting on quality of SPECT images has a great importance. In this study, we use the SIMIND MC simulation code to investigate the effect of a number of parameters on the quality of SPECT images, such as the arc of rotation, the number of angular views, the image matrix size, the pixel size in projection images, the effect of different collimators, the effect of use of filter in image reconstruction, and also the effect of applying the scatter correction method on ^{99m}Tc SPECT images.

Materials and Methods

In this study, we used SIMIND MC code (version 6.2, Lund, Sweden) for simulating two phantoms, the multiple spheres phantom (old Jaszczak program) and three-dimensional Nonuniform Rational B-spline-based CArdiac-Torso (3D-NCAT) phantom, to evaluate different factors affecting the quality of Technetium (Tc)-99 m SPECT images. The simulated SPECT system is including a cylindrical NaI (Tl) scintillation crystal (with energy resolution 10% full width at half maximum [FWHM] and intrinsic spatial resolutions 0.36 cm, at 140 keV) equipped by a low-energy high-resolution (LEHR) collimator.

Multiple-spheres simulation

The multiple-spheres phantom (old Jaszczak program) is a water-filled cylindrical phantom (diameter 20 cm, length 22 cm), including six spheres with diameters 3.2, 2.6, 2, 1.6, 1.3, and 1 cm. By using the SIMIND MC code, it is possible to simulate this phantom in two situations: (1) cold-spheres in hot-background and (2) hot-spheres in cold-background. The "hot" and "cold" refer to the presence and absence of the Tc-99m activity. Figure 1 illustrates the central cross-section of this phantom together with an arbitrary projection, sinogram and slice of the reconstructed image from this phantom. Actually, the Jaszczak phantom is a basic phantom used in many studies in the fields of nuclear medicine imaging, such as the studies related to evaluating the scatter correction methods in SPECT imaging.[15,16]

In this study, we use three mathematical criteria, including image contrast, signal-to-noise ratio (SNR) and relative noise of the background (RNB), for evaluation of the effect of different factors on the quality of SPECT images. These criteria are calculated as follows:[15]

$$Contrast = \frac{\overline{N}_B - \overline{N}_S}{\overline{N}_B} \times 100 \quad (1)$$

$$SNR = \frac{\overline{N}_B - \overline{N}_S}{\delta_B} \times 100 \quad (2)$$

$$RNB = \frac{\delta_B}{N_B} \quad (3)$$

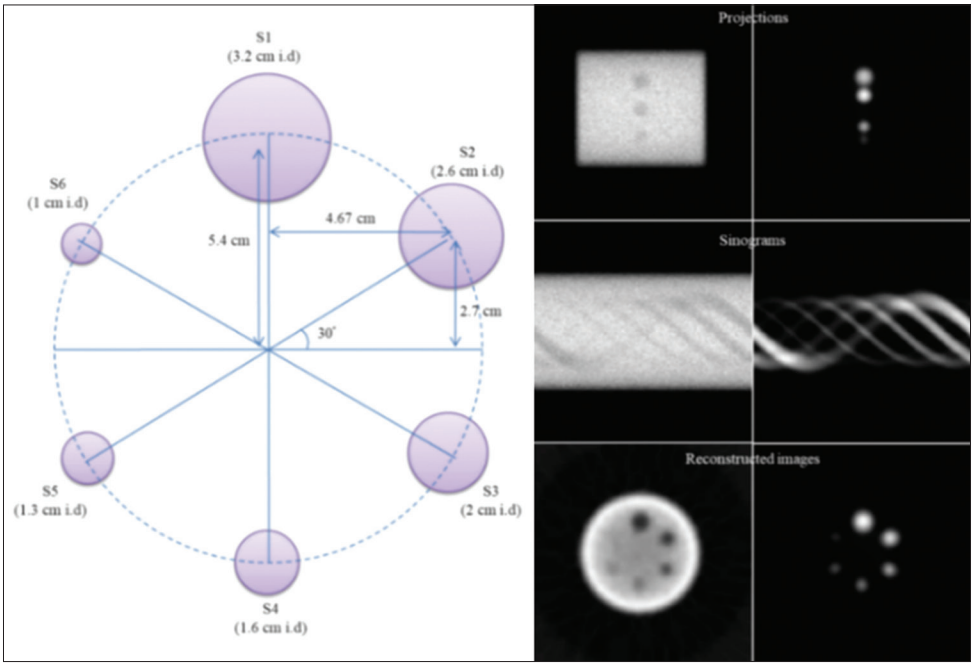

Figure 1: The illustration of cross-section of Jaszczak phantom including six spheres placed in a cylindrical phantom (left), and an arbitrary projection, sinogram and slice of the reconstructed image for cold-spheres in hot-background phantom (first column in right) and hot-spheres in cold-background phantom (second column in right)

$\overline{N}_S$ and $\overline{N}_B$ denote the mean counts in the region-of-interests (ROIs) defined into each of the spheres and into the background, respectively, and δ_B denotes the standard deviation of counts into ROI of the background.

In this study, we use a Tc-99 m activity equal to 5 mCi (5,000,000 photons/projection) for simulation of the Jaszczak phantom.

3D-NCAT simulation

In some cases, in addition to Jaszczak phantom, we used 3D-NCAT torso phantom[22,23] [Figure 2] that is a model of realistic activity distribution of the human body. The activity distributions used for the various organs of this phantom were according to the distributions defined by Segars and Tsui.[23] In this simulation, the number of 7142737 photons was acquired in each projection views. For evaluation of the images obtained from this phantom, the image contrast was defined by using a line profile through an arbitrary slice of the reconstructed image as follows:[16]

$$Contrast = \frac{MP - V}{MP + V} \quad (4)$$

where *MP* refered to the mean of two photopeaks, and *V* refer to valley between these two photopeaks in the line profile.

The projection images obtained from both Jaszak and 3D-NCAT phantoms were reconstructed by using the filtered back-projection (FBP) reconstruction algorithm. The programs related to the image reconstruction and the assessment criteria are written in MATLAB (version 7.5.0) environment (MathWorks, USA).

Results

The effect of the arc of rotation

For the investigation of the effect of the arc of rotation, we used a 180° rotation instead of a 360° rotation of camera. As shown in Figure 3, incomplete data acquisition results in distortion in the reconstructed images. Therefore, it seems to be necessary to use 360° rotation for SPECT imaging systems. However, there is an exception for cardiac SPECT imaging. Due to attenuation and scattering of the photons passing through the patient's chest, the projections acquired over the views left posterior oblique (180°) to ROA (360°) [Figure 4] include significant noise. Hence, the use of a 180° rotation instead of a 360° rotation results in improvement in the image contrast in cardiac SPECT imaging.[24] The image contrasts calculated by using the line profiles shown in Figure 5, confirmed this fact (contrast of 0.862 for 180° arc and 0.701 for 360° arc).

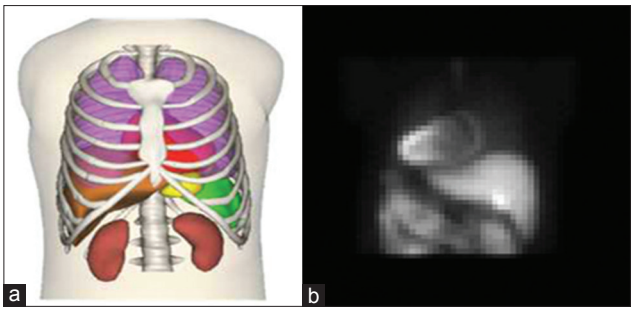

Figure 2: A total view of (a) 3D-NCAT phantom together with (b) an arbitrary projection of this phantom

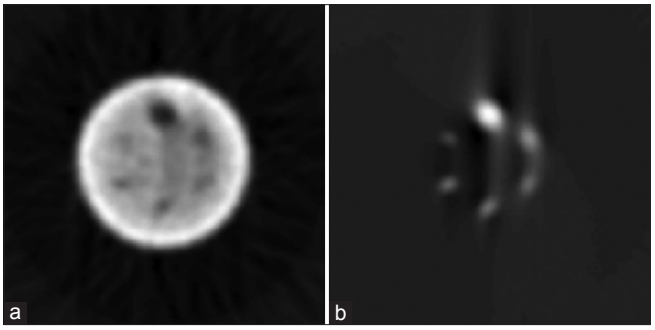

Figure 3: A slice of reconstructed image result from the acquisition of 64 projections (128 × 128 matrices) by a 180° rotation of the camera for (a) cold-spheres in hot-background phantom, and (b) hot-spheres in cold-background phantom

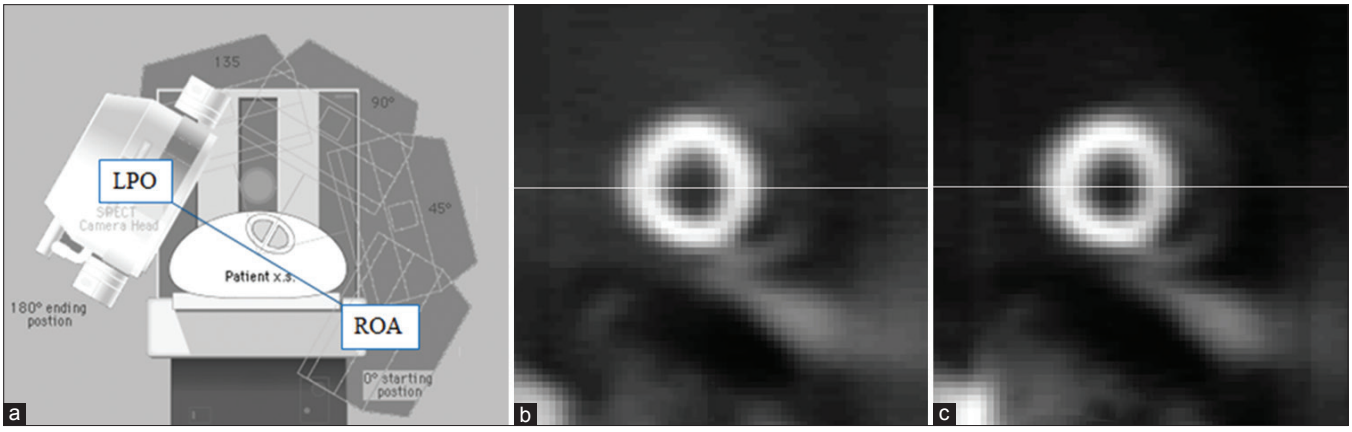

Figure 4: (a) The illustration of projection views in the cardiac imaging, and (b) an arbitrary slice of reconstructed image from 32 projections (64 × 64 matrices) acquired over a 180° arc, and (c) the corresponding slice of reconstructed image from 64 projections (64 × 64 matrices) acquired over a 360° arc

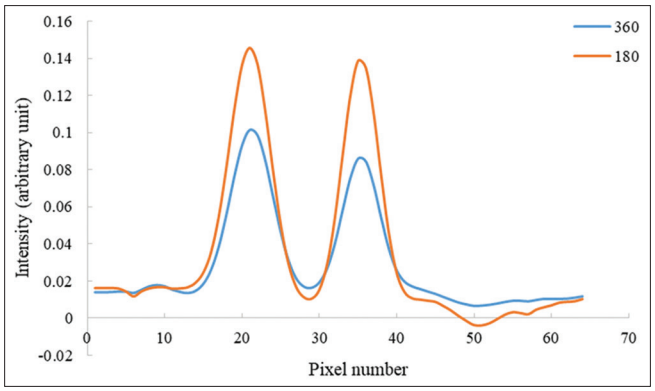

Figure 5: The line profiles from an arbitrary row [Figure 4] of the images reconstructed by using 180° and 360° arcs of rotation

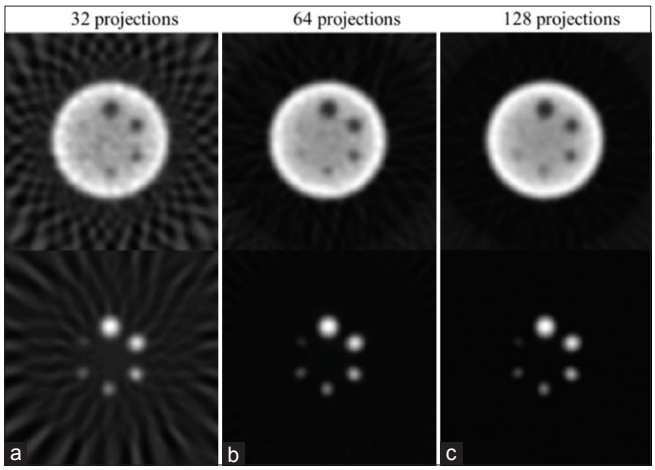

Figure 6: A slice of reconstructed image from cold-spheres in hot-background phantom (first row), and hot-spheres in cold-background phantom (second row) by using 128 × 128 projection image matrix with pixel size 0.3 cm and the number of (a) 32, (b) 64, and (c) 128 views

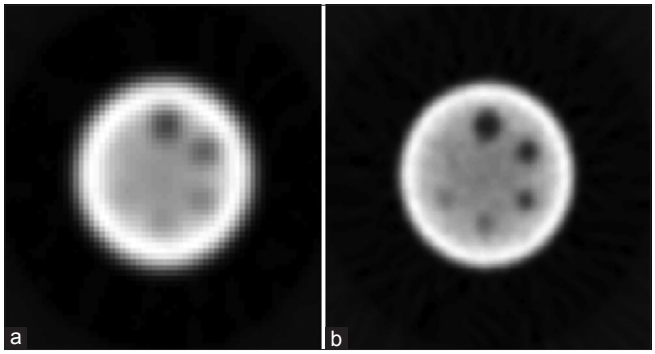

Figure 7: The reconstructed images from cold-spheres in hot-background phantom by using (a) a 64 × 64 image matrix with a pixel size 0.6 cm, and (b) a 128 × 128 image matrix with a pixel size 0.3 cm

The effect of the number of angular views

To investigate the effect of the number of angular views in SPECT imaging in a 360° rotation of the camera, we use 32, 64 and 128 views for a 128 × 128 projection image matrix (pixel size = 0.3 cm). As shown in Figure 6, for a 128 × 128 image matrix, if the number of views is lower than the image matrix size (128), the star artifacts may appear in the reconstructed image. Therefore, to avoid producing these artifacts, the number of views used for imaging should be at least equal to the projection image matrix size. Of course, it should be noted that the use of 128 views for a 128 × 128 image matrix leads to a significant increase in the imaging time and therefore, the probability of patient motion during the imaging. Hence, for preventing the appearance of the motion artifacts in reconstructed images, a 64 × 64 projection image matrix is usually used in clinical imaging.

The effect of image matrix size

The image matrices used in the nuclear medicine imaging have usually 64 × 64 and 128 × 128 sizes. For showing the effect of image matrix size on quality of SPECT images, we simulated the images in two situations:

1. By using a 64 × 64 projection image matrix with a pixel size 0.6 cm, and
2. By using a 128 × 128 projection image matrix with a pixel size 0.3 cm.

Figure 7 illustrates the results of these simulations. From this Figure, it is clear that the spatial resolution obtained from situation (1) is lower than that from situation, (2) image contrasts calculated for six cold-spheres show that only the first three largest spheres are distinguishable in the first situation. While for the second situation, all of the cold-spheres except the smallest sphere (spheres 6) are distinguishable. On the other hand, the RNB, in the first situation (0.0161) is approximately half of the second situation (0.0316). These results show that the use of a 128 × 128 projection image matrix leads to a higher spatial resolution compared to a 64 × 64 projection image matrix, but at the cost of reduction of SNR.

The effect of the presence of collimator

In the first stage, to show the effect of the presence of collimator on the quality of images obtained from SPECT imaging system, we performed simulation by using hot-spheres in cold-background phantom without the presence of any collimator. As shown in Figure 8, because of the acceptance of all of the photons arrived at the detector, regardless of their direction, the spatial resolution of the image reduces significantly. Therefore, it is necessary to use a suitable collimator depending on the purpose of imaging.

The collimators used in SPECT imaging are generally classified into three groups: High-resolution, high-sensitivity, and general-(all-) purpose collimators. High-resolution refers to the high ability of the imaging system for the detection of adjacent points, and high-sensitivity denotes to the high ability of the system for detection of the photons emitted by the source. The general-(all-) purpose collimators have the characteristics intermediate of high-resolution and high-sensitivity collimators.

Since Tc-99m is a radioisotope emitting low-energy gamma-rays, we investigate the effect of three collimators, low-energy high-resolution (LEHR), low-energy high-sensitivity (LEHS), and low-energy general-purpose (LEGP) on the Tc-99m SPECT images. Using the SIMIND MC code, it is possible to simulate different models of the collimators. In this study, we used GENERAL ELECTRIC (GE) collimator model. Figure 9 illustrates a slice of the reconstructed image from cold-spheres in hot-background phantom by using each of these collimators. Also, for a better comparison of the performance of three collimators, Tc-99m energy spectra obtained from the simulation of these collimators are given in Figure 10.

A number of spectral parameters obtained from the simulation of these collimators are given in Table 1. These parameters are including:

1. Compton area: The area under the energy spectrum (integral of simulated events) from energy 0 keV to lower energy limit (126 keV) of photopeak window
2. Photo area: The area under the energy spectrum from the lower energy limit (126 keV) to the upper energy limit (154 keV) of photopeak window
3. Pileup area: The area under the energy spectrum between upper energy limit (154 keV) of photopeak window to the highest energy of the spectrum
4. FWHM: This parameter is defined as FWHM of the photopeak at 140 keV
5. Collimator efficiency: This parameter is the geometric collimator efficiency that is defined as the

Table 1: The spectral parameters calculated by SIMulation of Imaging Nuclear Detector for cold-spheres in hot-background phantom in the simulation of GE-low-energy high-resolution, GE-low-energy general-purpose, and GE-low-energy high-sensitivity collimators

Parameter	GE-LEHR	GE-LEGP	GE-LEHS
Compton area ($\times 10^6$)	0.7112	1.417	3.246
Photo area ($\times 10^6$)	0.8665	1.727	3.956
Pileup area ($\times 10^6$)	0.0085	0.0171	0.0391
FWHM (keV)	17.057	17.045	16.864
Collimator efficiency	0.140	0.206	0.304
Sensitivity (cps/MBq)	36.6	72.9	167

GE: General Electric, LEHR: Low-energy high-resolution, LEGP: Low-energy general-purpose, LEHS: Low-energy high-sensitivity, FWHM: Full width at half maximum

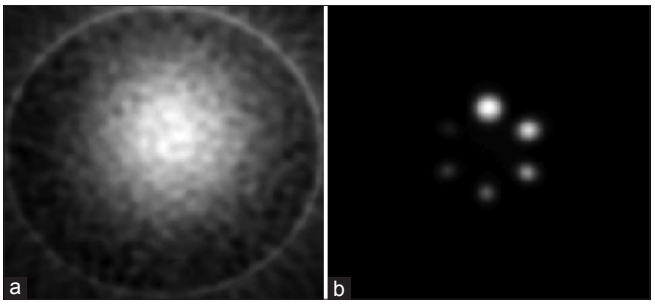

Figure 8: The reconstructed images from hot-spheres in cold-background phantom (a) without and (b) with simulation of the collimator

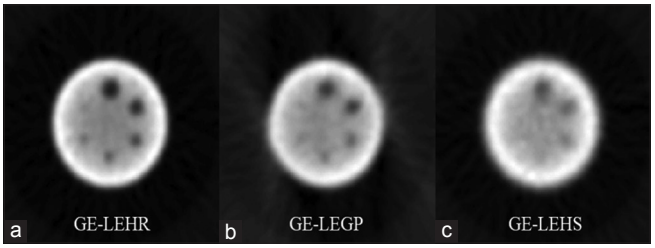

Figure 9: The reconstructed image from cold-spheres in hot-background phantom by simulating of three collimators: (a) GE-LEHR (b) GE-LEGP and (c) GE-LEHS

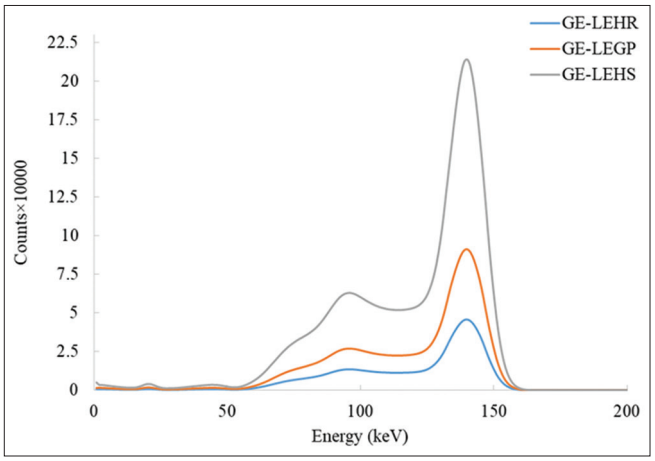

Figure 10: The Technetium-99m energy spectra obtained from the simulation of GE-LEHR, GE-LEGP, and GE-LEHS collimators

Table 2: The image contrasts and signal-to-noise ratios calculated for five spheres in reconstructed image of cold-sphere hot-background phantom with and without use of the filters

	None		Hann		Hamming		Cosine		Shepp-Logan		Ram-Lak	
	Contrast	SNR	Contrast	SNR	Contrast	SNR	Contrast	SNR	Contrast	SNR	Contrast	SNR
Sphere 1	−10.21	13.29	−61.56	19.47	−62.26	18.46	−65.91	15.73	−68.88	9.84	−70.37	7.88
Sphere 2	−8.54	11.12	−50.28	15.91	−51.40	15.24	−56.38	13.45	−61.59	8.80	−64.27	7.20
Sphere 3	−6.22	8.10	−36.34	11.49	−37.65	11.16	−43.60	10.40	−49.63	7.09	−52.71	5.90
Sphere 4	−3.32	4.32	−10.97	3.47	−11.36	3.37	−13.62	3.25	−15.19	2.17	−15.96	1.78
Sphere 5	−2.13	2.78	−6.00	1.90	−6.88	2.04	−9.80	2.34	−14.53	2.07	−17.04	1.91

Sphere 6 isn't recognizable. SNR: Signal-to-noise ratio

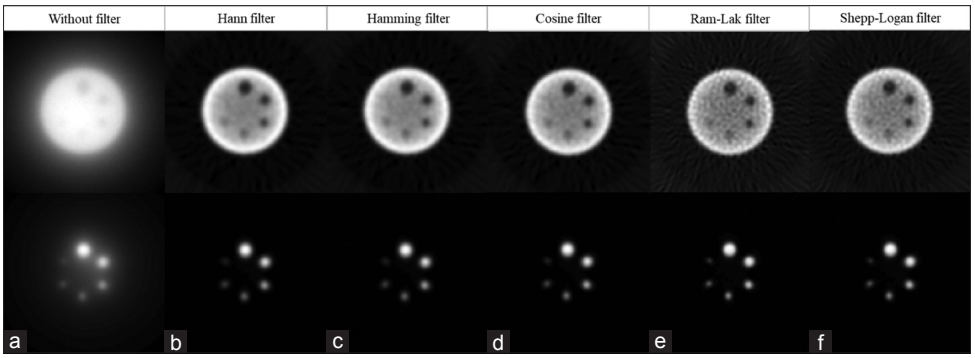

Figure 11: A slice of reconstructed image of cold-spheres in hot-background phantom (first row), and hot-sphere in cold-background phantom (second row), (a) without use of a filter, and by using five filters: (b) Hann (c) Hamming, (d) Cosine (e) Ram-Lak and (f) Shepp-Logan.

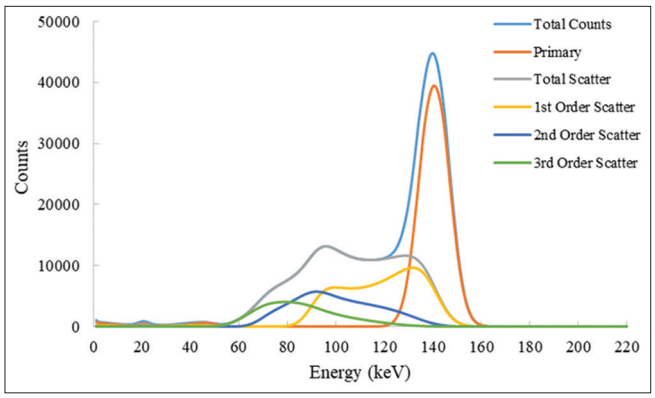

Figure 12: The energy spectrum of scatter, primary (nonscattered) and total counts together with the spectra of the first three scatter orders for Tc-99m radioisotope from the simulation cold-spheres in hot-background phantom

ratio of the number of photons passing through the interested collimator to the total number of emitted photons

6. Sensitivity: The ratio of count rate in the photopeak energy window to the activity used in the simulation.

The effect of use of the filters in reconstructed images

For evaluation of the effect of the use of the filter in the process of image reconstruction, we investigated two different situations:

1. The simple BP reconstruction without the use of any filter, and
2. The FBP reconstruction by using Ram-Lak, Hann, Hamming, Cosine, and Shepp-Logan filters. All of these filters are defined in the image reconstruction process which is programmed in MATLAB environment, with a cut-off frequency equal to 0.5 Hz for all of them.

The results of this simulation for cold-spheres in hot-background and hot-spheres in cold-background phantoms are shown in Figure 11. Furthermore, the image contrasts and SNRs calculated for the different situations shown in Figure 11, are given in Table 2.

From the data given in Table 2, it can be found that the use of a suitable filter in the image reconstruction process is necessary to improve both the image contrast and SNR. Among five

Table 3: The image contrasts and signal-to-noise ratios calculated for the cold spheres before and after applying the scatter correction

	Noncorrection		Corrected		Primary	
	Contrast	SNR	Contrast	SNR	Contrast	SNR
Sphere 1	71.88	23.00	64.52	21.66	85.57	23.14
Sphere 2	60.80	19.44	53.82	18.07	73.80	19.95
Sphere 3	43.44	13.89	39.23	13.17	51.29	13.87
Sphere 4	23.09	7.38	20.60	6.91	27.74	7.50
Sphere 5	6.40	2.05	4.72	1.58	9.53	2.58

SNR: Signal-to-noise ratio

filters evaluated in this study, the Ram-Lak filter and in lower rank, the Shepp-Logan filter, yield highest values for the image contrasts compared to other filters, but the SNRs obtained from these filters are significantly low, even lower than when is not used any filter. While the Hann filter and in lower rank, the Hamming filter, resulting in the highest SNRs or the lowest level of background noise (0.0316 for Hann filter and 0.0337 for Hamming filter compared to 0.892 for Ram-Lak filter and 0.699 for Shepp-Logan filter). The characteristics of Cosine filter are intermediate investigated filters. In this study, we used the Hann filter in the process of image reconstruction that shows a high degree of smoothing.[25]

The effect of detection of the scattered photons

One of the factors affecting on quality of SPECT images is the detection of Compton scattered photons into the photopeak energy window used in imaging. Since by using the simulation it is possible to distinguish the scattered photons from the primary (nonscattered) photons and produce individual images and energy spectra for each of them, simulation is a suitable tool for study in the field of scattering. Figure 12 shows the energy spectrum of total, primary and scattered counts together with the spectra of the first three scatter orders, obtained from the simulation of cold-spheres in hot-background phantom. The results of this simulation show that about 22% of photons detected into a 20% photopeak energy window are scattered photons that 86.5% of them are first-order scattered photons. The inclusion of these photons into the photopeak window results in the image blurring. Therefore, the use of a suitable

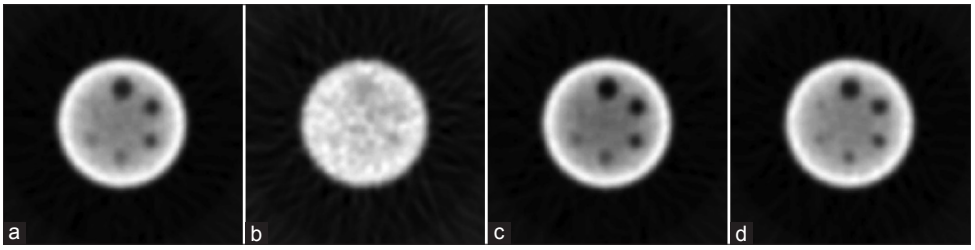

Figure 13: The cold-sphere images reconstructed from (a) total, (b) scatter, (c) primary counts together with (d) image corrected by dual-energy window method

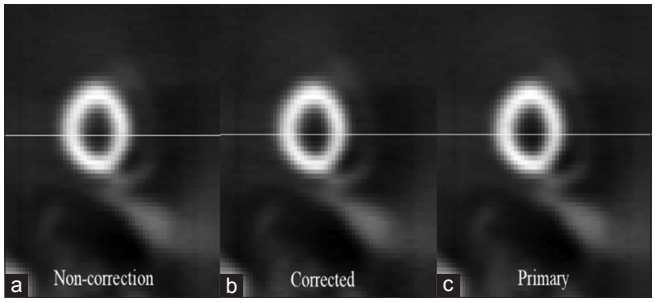

Figure 14: An arbitrary slice of reconstructed image from three-dimensional Nonuniform Rational B-spline-based CArdiac-Torso (3D NCAT) phantom in three situations: (a) non-correction (b) corrected by dual-energy window (DEW) method and (c) the image obtained from primary counts

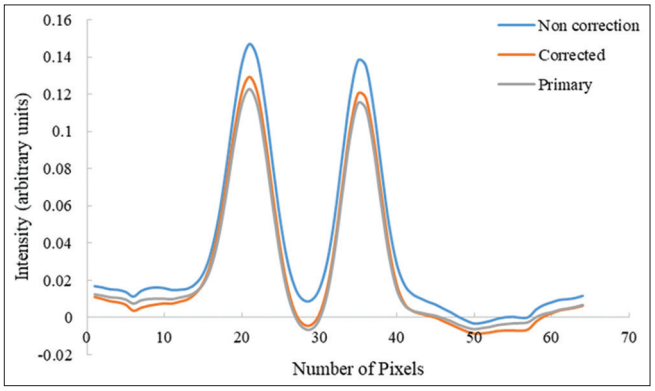

Figure 15: The line profiles obtained from an arbitrary row of the images reconstructed from 3D-NCAT phantom in three situations [Figure 14]

scatter correction method can help to increase the image contrast and therefore, improve the diagnostic accuracy.

One of the simplest and most effective methods proposed to reduce the contribution of scattered photons is the dual-energy window (DEW) method.[25] In this correction method it is assumed that the spatial distribution of scatter counts detected in the photopeak energy window (126–154 keV) is same with that for the total counts detected in a secondary energy window (92–125 keV) placed in Compton area of Tc-99 m energy spectrum:[14]

$$S_{pk}(i,j) = kT_c(i,j) \quad (5)$$

The "*k*" factor is determined by dividing pixel-to-pixel of the scatter projection of photopeak window (S_{pk}) to the projection of Compton window (T_C). Then by averaging "*k*" values obtained for different pixels (i, j), the calculated mean "*k*" value (=0.46) is used for scatter correction.[14,26] Figure 13 illustrates the cold-sphere images reconstructed from total, scatter and primary counts detected in 20% photopeak window together with the image corrected by DEW method. Also, the image contrasts and SNRs for six cold-spheres are given in Table 3. The results obtained from this simulation show that the use of the DEW scatter correction method results in improvement of the image contrasts with SNRs near to before the correction.

For more evaluation, we investigated the effect of this scatter correction method on the reconstructed images of 3D-NCAT phantom. Figure 14 illustrates an arbitrary slice of the reconstructed image of this phantom before and after scatter correction along with the image reconstructed from the primary photons. By using the line profiles shown in Figure 15, The contrast of images corrected by DEW method (=1.062) show a relative increase about 21.1% compared to the image contrast before the correction (=0.877).

Discussion and Conclusion

Since many researchers do not have access to the medical imaging systems and also, due to some limitations of the clinical imaging systems (e.g., lack access to the scattered and primary counts), and the risks of the radioactive sources for the human health, development of MC codes was a great step to increase and improve the studies in the different fields of the nuclear medicine imaging.

In this study, we used the SIMIND MC code dedicated to SPECT imaging, and also two simulated Jaszczak and 3D-NCAT phantoms for investigating several factors affecting on the quality of SPECT images.

The results of this study show that when the number of angular views is lower than image matrix size, it results in the appearance of artifacts in the reconstructed images. To prevent these artifacts, the number of acquired projections must be kept at least equal to image matrix size. Furthermore, by choosing a larger image matrix size and a smaller pixel size, the final reconstructed image would have higher spatial resolution with a higher level of the noise and a longer time required for imaging. On the other hand, except in cardiac imaging, data acquisition by using 180° rotation of camera results in some

of the anomalies in the reconstructed images compared to a 360° arc of rotation.

Also, for reducting the detection of scattered photons and preventing the production of the images with undesirable spatial resolution or degraded image contrast, it is necessary to use a detector system equipped with a suitable collimator and also use of a suitable filter in the image reconstruction process approporate to the purpose of imaging.

In final, presence of scattered photons into the used photopeak energy window is one of the essential problems in SPECT imaging that leads to blurring of the image. For resolving this problem, access to scattered counts and their spectrum can be a great help for scatter correction. The MC simulation codes provide this capability for researchers. Therefore, the simulation is a suitable tool for the studies related to scattering and also in the evaluation of scatter correction methods. The results obtained from this research show that the use of DEW scatter correction method improves the image contrast and therefore, diagnostic accuracy.

Financial support and sponsorship
Nil.

Conflicts of interest
There are no conflicts of interest.

References

1. Bridge P, Gunn T, Kastanis L, Pack D, Rowntree P, Starkey D, *et al*. The development and evaluation of a medical imaging training immersive environment. J Med Radiat Sci 2014;61:159-65.
2. Ljungberg M, Strand SE. A Monte Carlo program for the simulation of scintillation camera characteristics. Comput Methods Programs Biomed 1989;29:257-72.
3. Yanch J, Dobrzeniecki A, Ramanathan C, Behrman R. Physically realistic Monte Carlo simulation of source, collimator and tomographic data acquisition for emission computed tomography. Phys Med Biol 1992;37:853-70.
4. Thompson CJ, Moreno-Cantu J, Picard Y. PETSIM: Monte Carlo simulation of all sensitivity and resolution parameters of cylindrical positron imaging systems. Phys Med Biol 1992;37:731-49.
5. Zaidi H, Scheurer AH, Morel C. An object-oriented Monte Carlo simulator for 3D cylindrical positron tomographs. Comput Methods Programs Biomed 1999;58:133-45.
6. Reilhac A, Lartizien C, Costes N, Sans S, Comtat C, Gunn R, *et al*. PET-SORTEO: A Monte Carlo-based simulator with high count rate capabilities. IEEE Trans on Nucl Sci 2004;51:46-52.
7. Bielajew A, Hirayama H, Nelson W, Rogers D. History, Overview and Recent Improvements of EGS4, Technical Report. Ottawa, Canada: National Research Council; 1994.
8. Agostinelli S, Allison J, Amako K, Apostolakis J, Araujo H, Arce P, *et al*. Geant4: A simulation toolkit. Nucl Methods Instrum Phys Res A 2003;506:250-303.
9. Jan S, Santin G, Strul D, Staelens S, Assié K, Autret D, *et al*. GATE: A simulation toolkit for PET and SPECT. Phys Med Biol 2004;49:4543-61.
10. Briesmeister J. MCNP – A general Monte Carlo N-particle transport code", Technical Report. Los Alamos, NM, USA: Los Alamos National Laboratory; 1993.
11. Buvat I, Lazaro D. Monte Carlo simulations in emission tomography and GATE: An overview. Nucl Methods Instrum Phys Res 2006;569:323-9.
12. Ljungberg M, Strand SE, King MA. Monte Carlo Calculations in Nuclear Medicine Applications in Diagnostic Imaging. London: IOP Publishing; 1998.
13. Dewaraja YK, Ljungberg M, Fessler JA. 3-D Monte Carlo-Based Scatter Compensation in Quantitative I-131 SPECT Reconstruction. IEEE Trans Nucl Sci 2006;53:181.
14. Holstensson M, Hindorf C, Ljungberg M, Partridge M, Flux GD. Optimization of energy-window settings for scatter correction in quantitative (111) In imaging: comparison of measurements and Monte Carlo simulations. Cancer Biother Radiopharm 2007;22:136-42.
15. Asl MN, Sadremomtaz A, Bitarafan-Rajabi A. Evaluation of six scatter correction methods based on spectral analysis in (99m) Tc SPECT imaging using SIMIND Monte Carlo simulation. J Med Phys 2013;38:189-97.
16. Noori-Asl M, Sadremomtaz A, Bitarafan-Rajabi A. Evaluation of three scatter correction methods based on estimation of photopeak scatter spectrum in SPECT imaging: A simulation study. Phys Med 2014;30:947-53.
17. Rafati M, Rouhani H, Bitarafan-Rajabi A, Noori-Asl M, Farhood B, Ahangari HT. Assessment of the scatter correction procedures in single photon emission computed tomography imaging using simulation and clinical study. J Cancer Res Ther 2017;13:936-42.
18. Ahmadi S, Rajabi H, Sardari D, Babapour F, Rahmatpour M. Attenuation correction in SPECT during Image reconstruction using inverse Monte Carlo method a simulation Study. Romanian Rep Phy 2014;66:200-11.
19. Ljungberg M, Larsson A, Johansson L. A New Collimator Simulation in SIMIND Based on the Delta-Scattering Technique. IEEE Trans Nucl Sci 2005;52:1370-5.
20. Ljungberg M, Sjögreen-Gleisner K. The accuracy of absorbed dose estimates in tumours determined by quantitative SPECT: A Monte Carlo study. Acta Oncol 2011;50:981-9.
21. Pirayesh Islamian J, Bahreyni Toossi MT, Momennezhad M, Naseri S, Ljungberg M. Simulation of a quality control Jaszczak phantom with SIMIND Monte Carlo and adding the phantom as an accessory to the program. Iran J Med Phys 2012;9:135-140.
22. Segars WP, Lalush DS, Tsui BM. A realistic spline-based dynamic heart phantom. IEEE Trans Nucl Sci 1999;46:503-6.
23. Segars WP, Tsui BM. Study of the efficiency of respiratory gating in myocardial SPECT using the new 4D NCAT phantom. IEEE Trans Nucl Sci 2002;49:675-9.
24. Groch MW, Erwin WD. SPECT in the year 2000: Basic principles. J Nucl Med Technol 2000;28:233-44.
25. Lyra M, Ploussi A. Filtering in SPECT image reconstruction. Int J Biomed Imaging 2011;2011:1-14.
26. Jaszczak RJ, Greer KL, Floyd CE Jr., Harris CC, Coleman RE. Improved SPECT quantification using compensation for scattered photons. J Nucl Med 1984;25:893-900.